IEEE Access
Multidisciplinary | Rapid Review | Open Access Journal

Received February 25, 2022, accepted March 2, 2022, date of publication March 4, 2022, date of current version March 16, 2022.

Digital Object Identifier 10.1109/ACCESS.2022.3157050

Soft Switching Multiphase Interleaved Boost Converter With High Voltage Gain for EV Applications

NABIL A. AHMED[1], (Senior Member, IEEE), BADER N. ALAJMI[1], (Member, IEEE), IBRAHIM ABDELSALAM[2], (Senior Member, IEEE), AND MOSTAFA I. MAREI[3], (Senior Member, IEEE)

[1]Department of Electrical Engineering, College of Technological Studies, Public Authority for Applied Education and Training, Shuwaikh 70654, Kuwait
[2]Department of Electrical and Control, College of Engineering and Technology, Arab Academy for Science, Technology and Maritime Transport, Cairo 2033, Egypt
[3]Electrical Power and Machines Department, Faculty of Engineering, Ain Shams University, Cairo 11517, Egypt

Corresponding author: Nabil A. Ahmed (na.ahmed@paaet.edu.kw)

This work was supported in part by the Public Authority for Applied Education and Training (PAAET), and in part by the College of Technological Studies under Project TS-21-08.

ABSTRACT In this paper, a soft switching interleaved boost converter (SS-IBC) using auxiliary resonant circuit for electric vehicles (EV) applications is proposed. Several phases of the proposed converter can be connected to make a multiphase interleaved boost converter. The operation of multiphase interleaved boost converter is identical to that of the one phase boost converter. All phases are ideally identical with shifted control signals and are controlled by PWM control strategy of equal switching frequency and duty cycle. The proposed converter can be considered as a cost effective retrofit to the grid integrated battery charging applications. It affords a steady electrical power for the load not only from the utility or classical energy storage systems as batteries, but also from renewable energy systems like photovoltaic (PV), wind or fuel cell systems. An appropriate design example demonstrates the size of the design circuit components and parameters are investigated. Analysis, design, and simulation of the presented converter are verified using PSIM simulation software on an 8.2 kW setup system with a conversion efficiency more than 97% over a wide output power conversion range from rated power to a minimum power of 460 W with complete soft switching operation. The converter performance is also validated experimentally on a downsized hardware rated 1.0 kW and the maximum efficiency is found to be 98.78%.

INDEX TERMS Auxiliary resonant circuit, battery charger, electric vehicle, powertrain, interleaved boost converter, soft switching.

I. INTRODUCTION

Because of the increasing interest in environmental issues related to ever-increasing demand for energy, the depletion of fossil fuels and internal combustion engine (ICE) vehicles [1], there is a great interest in renewables, integrated distributed generators and electric propulsion. These realities demonstrate the growing market concern to electric vehicles (EVs) and hybrid EVs [2]. Corresponding to the demonstrated statistics, in 2050 there will be no ICE vehicles, and most vehicles will be either electric or plug-in hybrids electric (PHEV) [2]. Consequently, numerous authorities have incentivized both the progress and the purchase of EVs [2]. Therefore, EVs represent a great option as a mode of transportation, although some technological issues still must be overcome [2]. In the Europe Union, the transport sector is responsible for one quarter of the greenhouse gas emissions, becoming the second largest emitter of gases after energy sector. Therefore, the Europe Union has instituted a number of greenhouse gas reduction strategies, involving that ICE vehicles account for only half of the urban transport in 2030, and totally eliminated on 2050 [3].

The electric vehicle market is gradually demanding a range of more powerful powertrains to approach improved drivability better than or at least similar to ICE vehicles. For more electric power propulsion in EVs, battery EV (BEV),

The associate editor coordinating the review of this manuscript and approving it for publication was Jiann-Jong Chen.

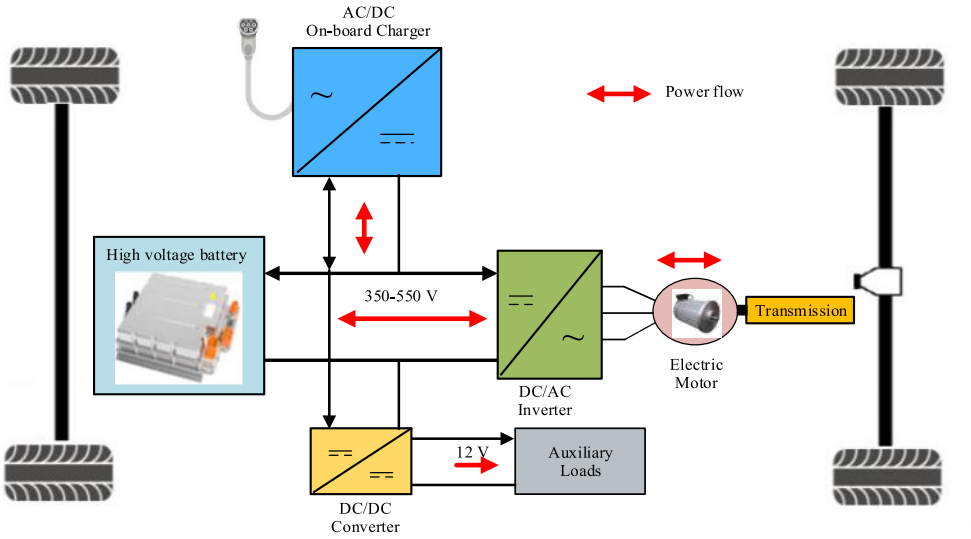

FIGURE 1. Block diagram of the battery electric vehicle powertrain.

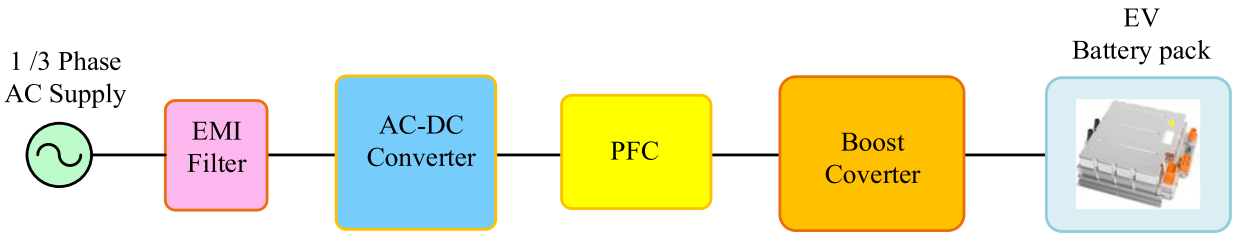

FIGURE 2. Level 1 on-board EV charger.

fuel cell EV (FCEV), HEVs and plug-in HEVs (PHEVs), a secondary high voltage battery pack must be installed to start the engine using the inverter. The high voltage battery pack is made up of multiple lithium-ion cells and stores the energy needs to run the vehicle. The use of a high voltage battery pack produces low current, high power density, and high torque while reducing the conduction losses [4]. However, it raises the cost, weight, and size of the entire system. Nevertheless, the boost converter is an additional component of the system that increases the conduction and switching losses especially at high power ratings, resulting in reduced power conversion efficiency. Therefore, some HEVs makers as Toyota hybrid system II, adopt the use of boost converters to boost the low battery voltage [5]. Fig. 1 shows the schematic diagram of the typical BEV powertrain. It consists of a high voltage battery pack, onboard battery charger, boost converters, electric motor and power management and control system.

Moreover, to gain widespread acceptance, EVs still face some important challenges such as supplementary cost, battery life, lack of charging infrastructure and issues related to battery chargers. Since EVs require electric power chargers rather than fuel filling, an additional crucial difficulty is the significant harmonics produced by EV chargers which have harmful effects on distribution networks [6]. This problem can be reduced by using active converters and power factor correction stages as well as high quality boost converters. Many car drivers find that charging their EV at home is more satisfactory than frequently going a gas station, saving time, effort as well as money. However, public charging stations for EV's are also becoming widespread, due to rapid growth in EV's market. This action creates a necessity to develop better EV chargers in terms of efficiency, durability, availability, reliability, and reduced price. Fig. 2 shows the block diagram of a level 1 EV charger as an example of on-board charger fed by one phase or three-phase power supply [7]. It consists of an EMI filter, AC-DC rectification stage, power factor correction stage and DC-DC boost conversion stage as an example of on-board power converter structure.

Numerous structures have been proposed in literature as isolating and non-isolating topologies for boost converters [8], [9]. The traditional boost structure which is the simplest topology is not cost effective in high power applications because of its limited voltage gain, lower efficiency, extreme duty cycle operation and high-voltage stress on the power semiconductor devices [10]. To cope with these difficulties, several techniques using magnetic coupling including coupling inductors or isolating transformers coupled inductors [9], [11], [12], switched capacitor, switched inductor and voltage doubles [13], [14]. However, such topologies are complex structures since it need various

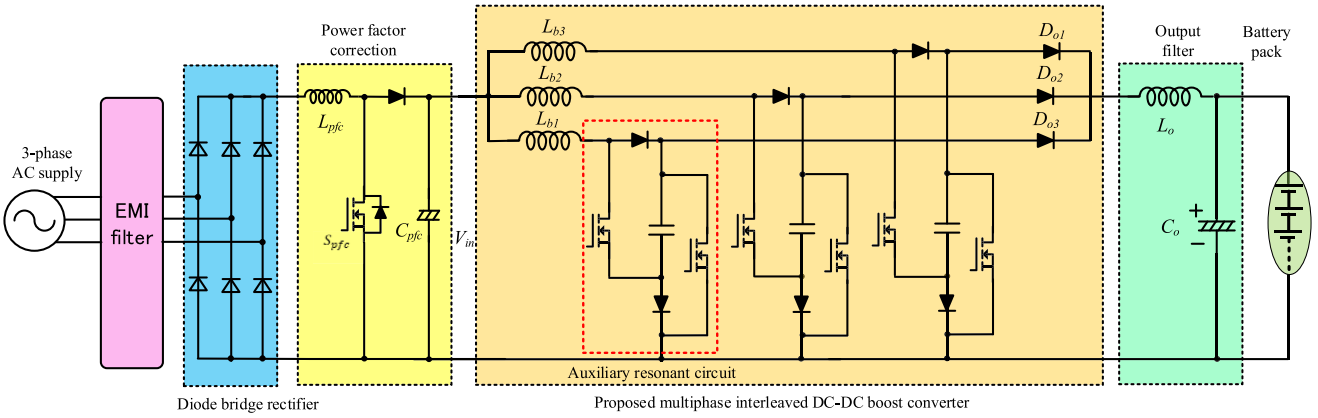

FIGURE 3. Proposed EV charger.

legs to attain a high voltage conversion ratio. Moreover, the leakage inductance of the coupled inductor increases the voltage stress and spikes on switches [15]. Several literatures work produce non-isolated structures [16] using a one switch, or produce various configurations based on traditional structures [13]. In [17], the combination of buck cand boost converters is employed to connect PV and battery systems with various types of applications.

During the past decade, various researchers have proposed various converters for decreasing current ripple and innovative DC-DC converter topologies [18], [19] including interleaved boost converters (IBC) [20]–[22]. IBCs are an encouraging interface between renewable energy sources such as fuel cells, PV, and the DC link of inverters. Due to interleaving process, IBCs present both lower current ripple at the supply side and lower voltage ripple at the load side [23]. The three-phase IBC is validated by an adjustment between size of the components, conversion efficiency, current ripple, switch count, and cost [20]. The IBC permits acting to the exciting difficulties in FCEV applications in terms of power density, conversion efficiency, and current ripple. Therefore, in high power applications, interleaving topologies are commonly implemented as an effective solution to overcome the problem of current ripple, decrease element size, increase power rating, enhance dynamic response, and achieve high conversion efficiency [24]–[29]. These new structures are good candidates towards highly efficient vehicle powertrain and chargers. Nevertheless, more advances towards improved outcomes are still widely open and promising.

The auxiliary resonant circuit is an effective technique that is widely used in switching converters to overcome the disadvantages of hard switching PWM boost dc-dc converters due to their high efficiency and high scalability properties. It enables a wide range of soft switching operations under continuous and discontinuous current modes of operation without any circulating currents. In addition, the current and voltage stresses in the switching devices can also be reduced resulting in using high switching frequency, reduced power loss and high conversion efficiency. Furthermore,

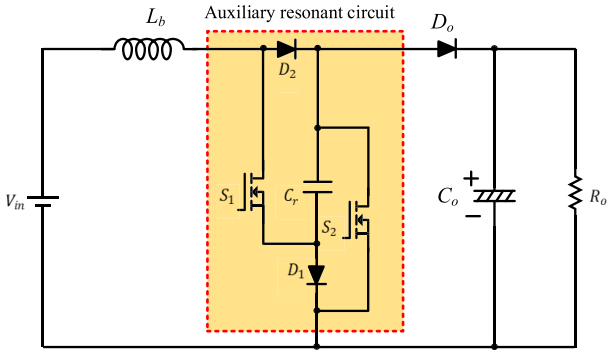

FIGURE 4. One phase of proposed SS-IBC.

soft-switching converters can be usefully extended for the interleaved circuit topology, that effectively reducing the input current ripple and reducing the size of the circuit components and increasing the converter power rating.

In this paper, a new soft switching multiphase interleaved boost converter employing an auxiliary resonant circuit for EV applications is presented. Most important advantages of the proposed interleaved converter include: 1) A wide soft switching power control range; 2) A reduction of the ripple currents by an interleaved operation; 3) A minimization of conduction power loss by discontinuous current operation in the input side; and 4) A high voltage conversion ratio. Due to these features, the proposed converter is very convenient for high volage batteries in EV applications and low voltage sources as PV and fuel cell systems, which require high-voltage conversion capability. The paper is organized as follows: proposed soft switching interleaved boost converter (SS-IBC) topology including configuration, operation performance and analysis is described in section II. Detailed steady-state analysis, performance equations and the operation modes with their equivalent circuits and voltage and current waveforms in one switching cycle are conducted in section III. Design consideration of circuit parameters is carried out in section IV. Simulation results and real measurements using experimental setup are given

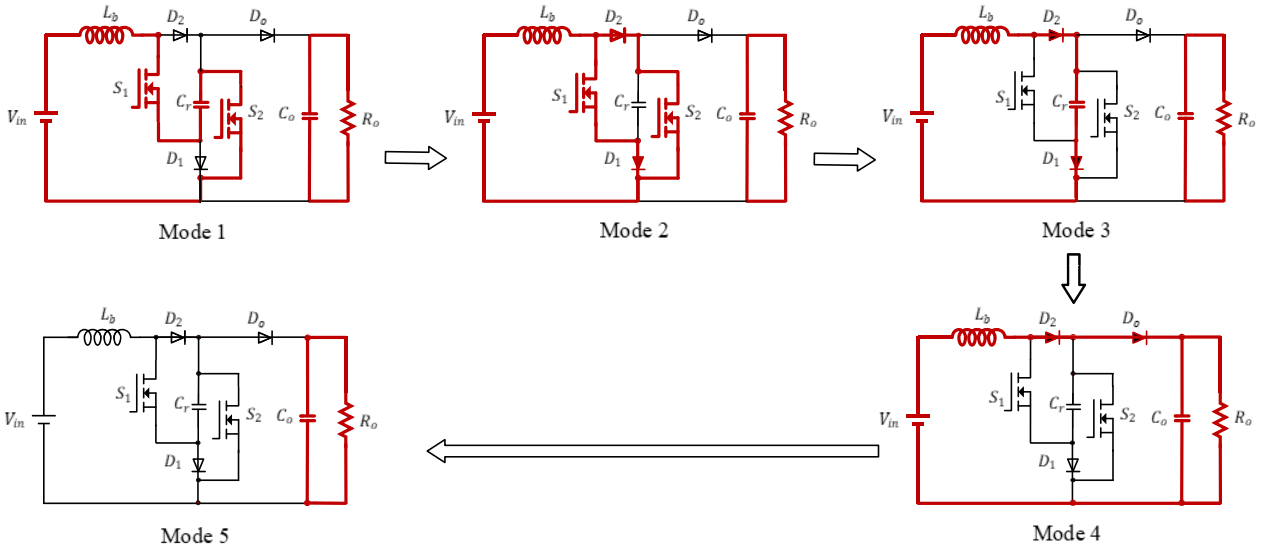

FIGURE 5. Equivalent circuit and operation modes during one switching cycle.

in sections V and VI, respectively. Conclusion remarks are given in section VII.

II. PROPOSED SOFT SWITCHING INTERLEAVED BOOST CONVERTER

A. CIRCUIT DESCRIPTION

Fig. 3 illustrates the circuit configuration of the typical EV charger with the proposed SS-IBC employing auxiliary resonant circuit. Fig. 4 shows the one phase of proposed soft switching interleaved boost converter. One auxiliary active switch (S_2), one resonant capacitor (C_r) and two diodes (D_1 and D_2) are added to the conventional soft switching boost converter. The proposed IBC can be operated as a bidirectional converter if the output diode D_o and diode D_2 are replaced by active switches. In addition to the simplicity, the essential characteristic of the proposed converter is the lower current and voltage stress on the active and auxiliary switch. The utilization of proposed resonance circuit enables zero voltage switching (ZVS) for the switches and diodes. Thus, resulting in higher conversion efficiency. Several phases of the proposed converter can be linked in parallel to develop a multiphase interleaved boost converter. The operation of the proposed multiphase interleaved converter is identical to that of the one phase boost converter. All phases are ideally identical with shifted control signals and are controlled by PWM control strategy of the equal switching frequency and duty cycle. The PWM switching function for all phases are equal, but phase shifted by 360/N degrees, where N is the number of phases. The proposed converter can be considered as a cost effective retrofit of the existing boost converters. It offers a stable high DC voltage power supply for the load not only from the utility or conventional energy storage systems as battery, but also from renewable resources like PV, FC or wind systems. Analysis, design, and simulation of the proposed converter are carried out using PSIM simulation software and verified experimentally on a hardware setup. In addition, an appropriate design example to demonstrate the sizing of the required components and circuit parameters is investigated. Moreover, comparison of power conversion efficiency and the ripple factor of the input current between the proposed SS-IBC and conventional hard switching converter are considered. A high and steady conversion efficiency more than 97% is obtained and the ripple factor is well improved as the number of interleaved phases increases. Furthermore, the simulation and computed voltage and current waveforms are validated experimentally.

B. OPERATION PRINCIPLES AND OPERATION MODES

The detailed analysis of the converter is conducted in discontinuous conduction mode (DCM) under steady state operation condition. To facilitate the analysis, all power switches and passive elements are assumed ideal. The switching loss and internal resistance of inductor and capacitor are considered negligible. The operation modes are divided into five operation modes during each switching cycle. The equivalent circuit with the current paths during each mode are depicted Fig. 5, while the relevant voltage and current waveforms during each operation mode are illustrated in Fig. 6.

Mode 1 ($t_o \leq t < t_1$): Before the starting of mode 1, the resonant capacitor C_r is initially charged up to the output voltage V_0 and the boost inductor current i_{Lb} is zero. Mode 1 starts when the main active switch S_1 and the auxiliary active switch S_2 are simultaneously turned-on at $t = t_o$. The boost inductor current i_{Lb} and the switches currents i_{s1}, i_{s2} start to increase progressively from zero initial value and the capacitor starts to discharge gradually from V_0 to zero. Therefore, both active switches S_1 and S_2 are turned-on at zero current switching (ZCS) conditions. By assuming the time origin $t_o = 0$ for simplicity, the resonant capacitor

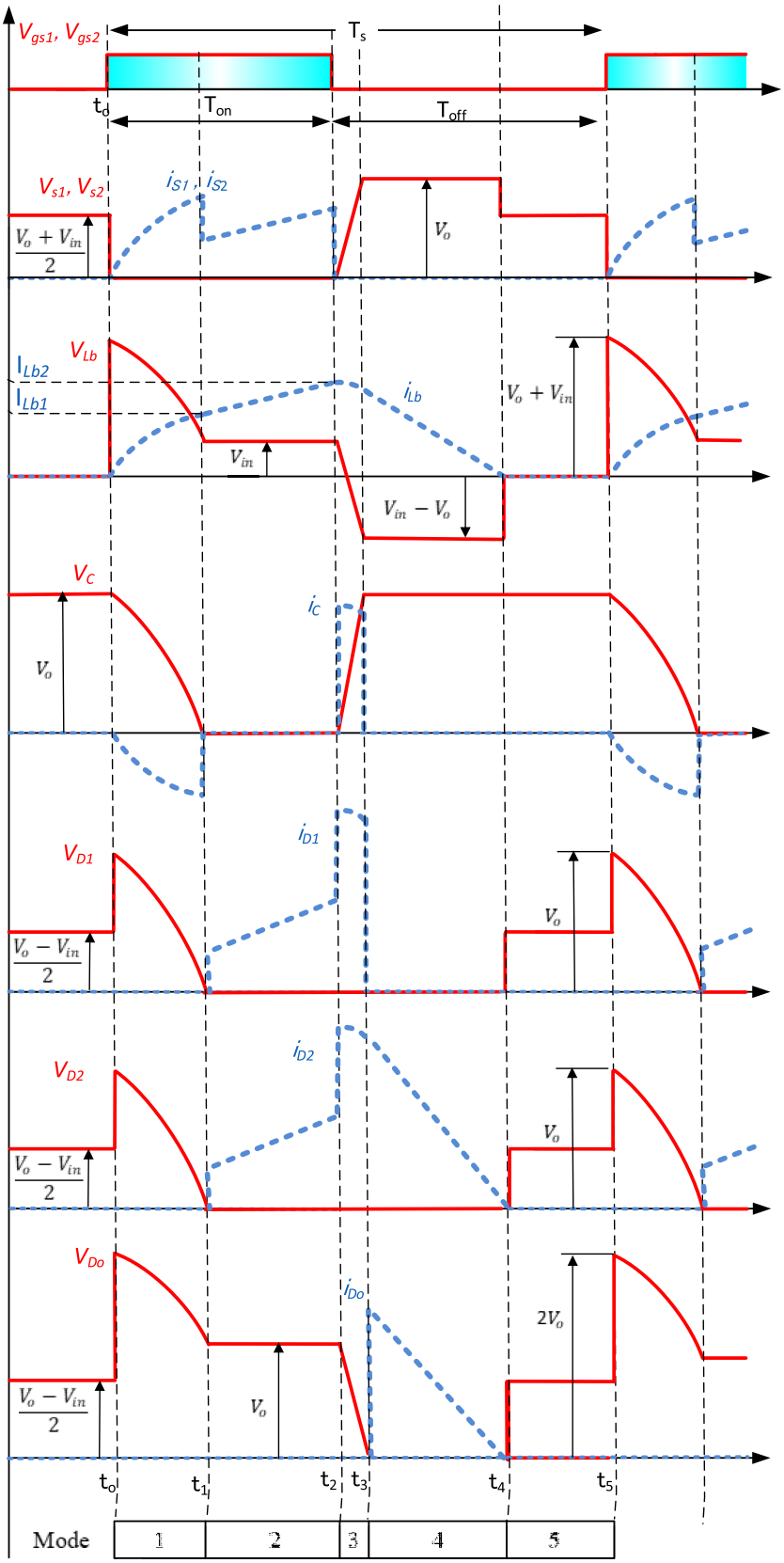

FIGURE 6. Relevant voltage and current waveforms during one switching cycle.

voltage, the boost inductor voltage, and switches currents can be given as follows:

$$v_{cr}(t) = (V_{in} + V_0)\cos(\omega_r t) - V_{in} \quad (1)$$

$$v_{Lb}(t) = (V_{in} + V_0)\cos(\omega_r t) \quad (2)$$

$$i_{Lb}(t) = i_{s1}(t) = i_{s2}(t) = (V_{in} + V_0)\sqrt{\frac{C_r}{L_b}}\sin(\omega_r t) \quad (3)$$

where ω_r is the angular resonance frequency and is defined as:

$$\omega_r = \frac{1}{\sqrt{L_b C_r}} \quad (4)$$

Mode 1 is completed at time t_1 when the resonant capacitor is totally discharged to zero and the boost inductor current reaches the value I_{Lb1} at the end of this mode.

$$t_1 = t_o + \sqrt{L_b C_r}cos^{-1}\left(\frac{V_{in}}{V_{in} + V_0}\right) \quad (5)$$

$$I_{Lb1} = i_{Lb}(t_1) = \left(\sqrt{V_o^2 + 2V_0 V_{in}}\right)\sqrt{\frac{C_r}{L_b}} \quad (6)$$

Mode 2 ($t_1 < t < t_2$): This mode is the boost inductor energy charging mode, and it is started when the voltage across the resonant capacitor reaches zero at time t_1. When the resonant capacitor is fully discharged at time t_1, the auxiliary diodes D_1 and D_2 become forward biased and start to be conducting. The boost inductor voltage equals the supply voltage, the resonant capacitor voltage is kept at zero value and the boost inductor current is equally divided to the parallel paths $(S_1 - D_1)$ and $(S_2 - D_2)$ and it increases linearly as:

$$v_{cr}(t) = 0 \quad (7)$$

$$v_{Lb}(t) = V_{in} \quad (8)$$

$$i_{Lb}(t) = \frac{V_{in}}{L_b}(\mathrm{t} - t_1) + \left(\sqrt{(V_o^2 + 2V_0 V_{in})}\right)\sqrt{\frac{C_r}{L_b}} \quad (9)$$

$$i_{s1}(t) = i_{s2}(t) = \frac{i_{Lb}(t)}{2} \quad (10)$$

This mode is terminated when the main switch S_1 and the auxiliary switch S_2 are simultaneously turned-off at time t_2.

$$t_2 = t_o + DT_s \quad (11)$$

where D is the duty cycle of the main and auxiliary switches S_1, S_2.

The boost inductor current reaches I_{Lb2} at the end of this mode.

$$I_{Lb2} = i_{Lb}(t_2) = \frac{V_{in}}{L_b}(DT_s - t_1) + \left(\sqrt{V_o^2 + 2V_0 V_{in}}\right)\sqrt{\frac{C_r}{L_b}} \quad (12)$$

$$I_{Lb2} = \frac{V_{in}}{L_b}\left(DT_s - \sqrt{L_b C_r}cos^{-1}\left(\frac{V_{in}}{V_{in} + V_0}\right)\right) + \left(\sqrt{V_o^2 + 2V_0 V_{in}}\right)\sqrt{\frac{C_r}{L_b}} \quad (13)$$

Mode 3 ($t_2 < t < t_3$): This mode begins when the main switch S_1 and the auxiliary switch S_2 are simultaneously turned off at time t_2, the resonance starts in the loop contains input voltage V_{in}, boost inductor L_b, diode D_2, resonant capacitor C_r and diode D_1. The voltage across the main switch S_1 and the auxiliary switch S_2 increase gradually from zero due to the existence of the resonant capacitor C_r. Therefore, the main and the auxiliary switches $S_1 S_2$ are turned-off at zero voltage switching (ZVS). Moreover, the voltage across the auxiliary diodes D_1 and D_2 are zero, therefore D_1 and D_2 are also turned-on at ZVS. The voltage and current relations are as follows:

$$v_{Lb}(t) = V_{in}\cos\omega_r(t - t_2) - \sqrt{\frac{L_b}{C_r}}I_{lb2}\sin\omega_r(t - t_2) \quad (14)$$

$$v_{cr}(t) = -V_{in}(1 - \cos\omega_r(t - t_2)) + \sqrt{\frac{L_b}{C_r}}I_{lb2}\sin\omega_r(t - t_2) \quad (15)$$

$$i_{Lb}(t) = \sqrt{\frac{C_r}{L_b}}V_{in}\sin\omega_r(t - t_2) + I_{lb2}\cos\omega_r(t - t_2) \quad (16)$$

During this mode the boost inductor current reaches its maximum value that is given by

$$I_{Lb}max = \sqrt{\frac{C_r}{L_b}V_{in}^2 + I_{Lb2}^2} \quad (17)$$

The boost inductor current can be simplified to:

$$i_{Lb}(t) = I_{Lb}max\sin\left\{\omega_r(t - t_2) + \tan^{-1}\frac{\sqrt{\frac{L_b}{C_r}}I_{Lb2}}{V_{\mathrm{in}}}\right\} \quad (18)$$

During mode 3, the resonance capacitor voltage increases gradually from zero and this mode maintains till the resonance capacitor voltage $v_{cr}(t)$ reaches the output voltage V_0 and the boost inductor voltage reaches a negative voltage equals $(V_{\mathrm{in}} - V_o)$ at time t_3.

$$t_3 = t_o + DT_s + \sqrt{L_b C_r}\left\{\sin^{-1}\frac{V_o + V_{\mathrm{in}}}{(V_{in}^2 + \frac{L_b}{C_r}I_{Lb2}^2)} - \tan^{-1}\frac{V_{\mathrm{in}}}{\sqrt{\frac{L_b}{C_r}}I_{Lb2}}\right\} \quad (19)$$

$$I_{Lb3} = \sqrt{\frac{C_r}{L_b}}V_{in}\sin\omega_r(t_3 - DT_s) + I_{lb2}\cos\omega_r(t_3 - DT_s) \quad (20)$$

Mode 4 ($t_3 < t < t_4$): This mode is the energy discharging mode, and it begins when the resonance capacitor voltage $v_{cr}(t)$ reaches the output voltage V_0 at time t_3. At this moment, the conduction of diodes D_1 and D_2 is ended and they turned-off at ZVS. The main and auxiliary switches are in off state, and the accumulated energy stored in the boost inductor is transferred to the load via the output diode D_o. During mode 4, the boost inductor current

gradually decreases and finally reaches zero at time t_4. The resonance capacitor and the boost inductor voltages are kept at V_0 and $(V_{\text{in}} - V_o)$; respectively. The voltage and current relations during mode 4 are as follows:

$$v_{cr}(t) = V_o \tag{21}$$
$$v_{Lb}(t) = V_{in} - V_o \tag{22}$$
$$i_{Lb}(t) = \frac{V_{in} - V_o}{L_b}(t - t_3) + I_{Lb3} \tag{23}$$
$$t_4 = t_3 + \frac{L_b I_{Lb3}}{V_o - V_{\text{in}}} \tag{24}$$

Mode 5 ($t_4 < t < t_5$): During mode 5, the boost inductor current is zero and the output current takes its path through the output capacitor C_o. The boost inductor current holds zero value till the beginning of the next switching cycle when the switches S_1 and S_2 are tuned-on again at the t_5.

$$v_{cr}(t) = V_o \tag{25}$$
$$v_{Lb}(t) = 0 \tag{26}$$
$$i_{Lb}(t) = 0 \tag{27}$$

The voltage gain (V_o/V_{in}) of the proposed converter can be obtained from the volts balance equation of the boost inductor voltage through one complete switching period. Using the volt-second balance equation during one switching period, the mean value of the boost inductor voltage $V_{lb,dc}$ should be zero. Therefore, average boost inductor voltage is given by:

$$V_{Lb,dc} = \frac{1}{T_s}\int_0^{T_s} v_{Lb}(t) = 0 \tag{28}$$
$$V_{Lb,dc} = \sqrt{L_b C_r}\left(V_o^2 + 2V_o V_{in}\right) + V_{in}(DT_s - t_1) - L_b I_{Lb2} = 0 \tag{29}$$

The average input current $I_{in,dc}$ can be obtained by integrating $i_{Lb}(t)$ given by equations (3), (9), (16), (23) and (27) during each operating mode as follows:

$$I_{in,dc} = \frac{1}{T_s}\int_0^{T_s} i_{Lb}(t) \tag{30}$$
$$I_{in,dc} = \frac{1}{T_s}\left\{\begin{array}{l} C_r V_o + \dfrac{V_{\text{in}}}{2L_b}(t_2 - t_1)^2 + I_{Lb1}(t_2 - t_1) \\ - C_r V_{\text{in}}(\cos(w(t_2 - t_1)) - 1) \\ + I_{Lb2}\sqrt{L_b C_r}(\sin(w(t_2 - t_1)) \\ + \dfrac{L_b I_{Lb3}^2}{2(V_o - V_{in})} \end{array}\right\} \tag{31}$$

Equation (31) can be simplified as:

$$I_{in,dc} = \frac{V_o}{T_s(V_o - V_{in})}\left\{2C_r V_o + \frac{V_{\text{in}}}{2L_b}(t_2 - t_1)^2 + I_{Lb1}(t_2 - t_1)\right\} \tag{32}$$

The input power can be given by

$$P_{in} = V_{in} I_{in,dc} = \frac{V_o V_{in}}{T_s(V_o - V_{in})}\left\{2C_r V_o + \frac{V_{\text{in}}}{2L_b}(t_2 - t_1)^2 + I_{Lb1}(t_2 - t_1)\right\} \tag{33}$$

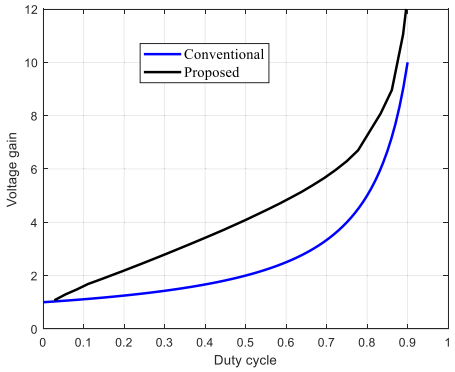

FIGURE 7. Comparison between voltage gain of proposed and conventional converter: $L_b = 50\ \mu H$, $C_r = 32\ nF$, $f_s = 40\ kHz$.

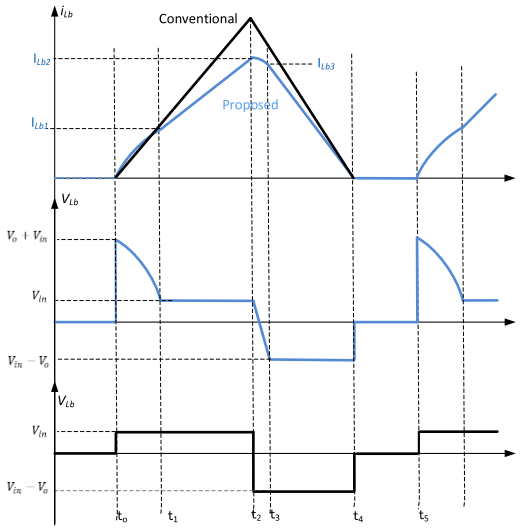

FIGURE 8. Comparison between voltage and current waveforms of proposed and conventional converter.

Equation (29) is an implicit relationship in the voltage gain of the proposed boost converter and by solving it numerically, the voltage gain can be obtained and compared to that of the standard boost converter. The comparison between the voltage gain of the proposed and standard boost converter is given in Fig. 7. It is clear that the proposed boost converter has a high voltage gain compared to the standard one. Comparison between voltage and current waveforms of the proposed and conventional converter are depicted in Fig. 8. Equations (1)-(27) have been programed and the computed voltage and current waveforms are illustrated in Fig. 9 which are identical to the expected voltage and current waveforms presented in Fig. 6.

III. DESIGN OF CIRCUIT PARAMETERS

The values of the boost inductor L_b and resonant capacitor C_r of the proposed soft switching boost converter are selected according to the maximum and the minimum output power corresponding to the maximum and minimum duty cycles, D_{max} and D_{min} respectively. These values determine the range of the soft switching control of output power. Increasing the

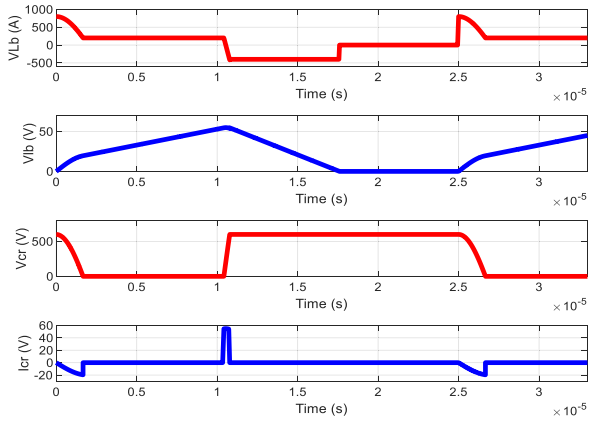

FIGURE 9. Computational results of boost inductor and resonant capacitor voltage and current waveforms.

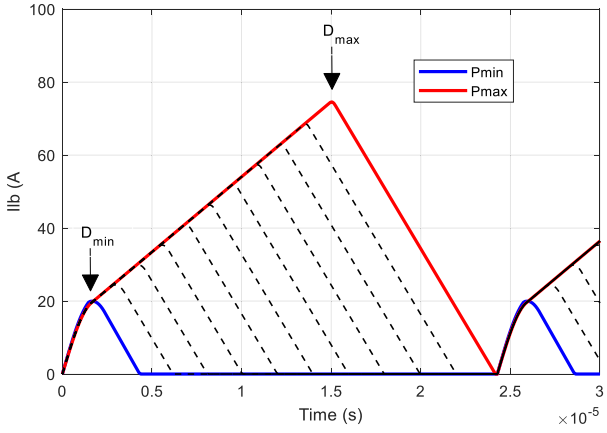

FIGURE 10. Effect of duty cycle on the boost inductor current.

value of boost inductor leads to continuous current operation so that the inductor current does not reach zero in mode 4. Therefore, the switches do not turn-on at ZCS. On the other hand, increasing the size of the resonant capacitor leads to the resonant capacitor not being fully discharged at the end of mode 1. This action makes it have a residual voltage and this voltage continues until the end of mode 2. This in turn leads to the fact that the two active switches S_1 and S_2 do not turn off at ZVS. Consequently, the values of the boost inductor and resonant capacitor should be designed according to these principles.

Fig. 10 depicts the boost inductor current at different duty cycles ranging from minimum duty cycle D_{min} to maximum duty cycle D_{max}. The value of the boost inductor achieve soft switching operation at maximum power operation is determined from zero-current crossing in mode 4. At this condition, mode 5 disappears and mode 4 ends exactly at the beginning of the next switching cycle (critical discontinuous operation). Therefore, to maintain soft switching operation at maximum power, the maximum interval time of mode 4, $t_{4,max}$, should be smaller than or equal one switching period T_s.

$$t_{4,max} \leq T_s \tag{34}$$

In the same way, at minimum power, the minimum interval time of mode 4 should be maintained greater than or equal to a minimum value, $t_{4,min}$, to allow the resonant capacitor to be fully discharged before the zero crossing of the boost inductor current.

Therefore, the condition of soft switching operation should satisfy the following condition:

$$t_{4,min} < t_4 = T_s \tag{35}$$

From Fig. 10, it is clear that the output power of the proposed SS-IBC can be regulated by controlling the duty cycle of the main and auxiliary switches. With an increase in the duty cycle, the output power grows, and with a decrease in the duty cycle, the output power decreases. The variations of the boost inductor current at different values of the resonant capacitor and boost inductor values while maintaining soft switching operation conditions are given in Figs. 11 and 12, respectively. From Fig. 11(b), decreasing the value of the resonant capacitor results in low value of minimum power limit and increasing the soft switching area. However, small values of resonant capacitor led to a high voltage change rate (dv/dt) on the active switches at turn-off transition.

At minimum power, $P_{in,min}$, operation, the second and third terms in equation (33) are too small and can be neglected. Therefore, $P_{in,min}$ can be simplified to:

$$P_{in,min} = V_{in} I_{in,dc,min} = \frac{2C_r V_{in} V_o^2}{T_s(V_o - V_{in})} \tag{36}$$

A minimum power of 460 W is selected in the design of the proposed soft switching converter and the value of the resonant capacitor can be calculated using (36) as 32 nF. This value of minimum power is selected to be the minimum power under complete soft switching operation conditions and the converter is still capable to operate at small power but without soft switching operation. From Fig. 12(b), as the value of the boost inductor increases, the peak value of the boost inductor current decreases but at the expense of the lengthen of the interval time of mode 4. This action may lead to continuous current operation and the loss of soft switching operation. A value of 50 μH for the boost inductor is found to be proper to keep soft switching operation at maximum output power of 8.2 kW. Fig. 13 illustrates the soft switching operation range as a function of the resonant capacitor at a boost inductor of 50 μH.

The peak inductor current is the sum of the average input current plus one-half of the peak-peak ripple and it can be expressed as follows:

$$\Delta I = 2(I_{Lb,PK} - I_{in,dc}) \tag{37}$$

The formula for ripple factor is:

$$Ripple\ factor = \frac{\Delta I}{I_{in,dc}} \tag{38}$$

IV. SIMULATION RESULTS

The proposed soft switching boost converter and its multiphase interleaved converter have been simulated using

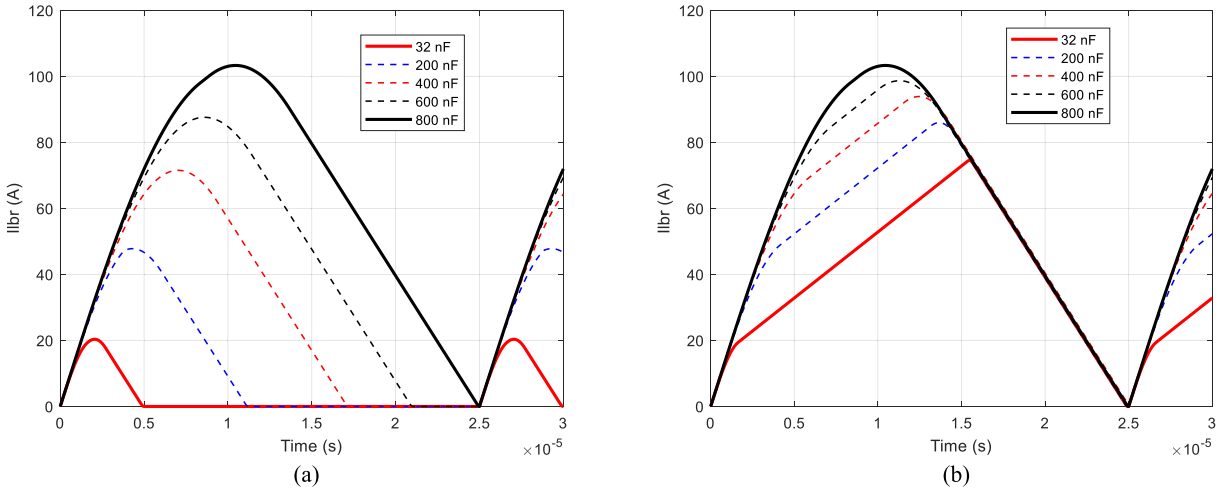

FIGURE 11. Effect of the resonant capacitor on the boost inductor current at maximum and minimum output power, $L_b = 50\ \mu H$: (a) Maximum power, (b) Minimum power.

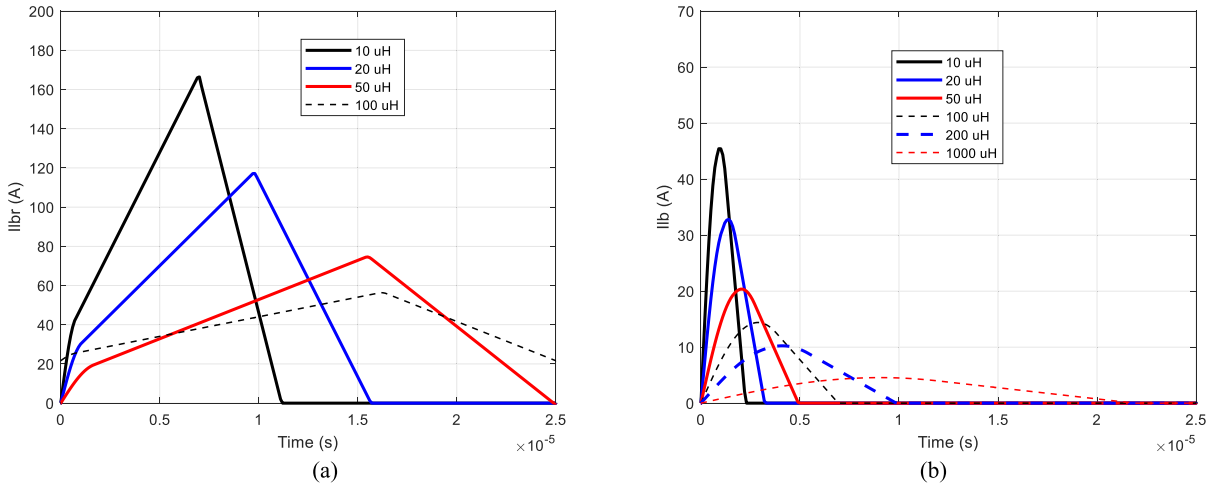

FIGURE 12. Effect of the boost inductor on the boost inductor current at maximum and minimum output power, $C_r = 32\ nF$: (a) Maximum power, (b) Minimum power.

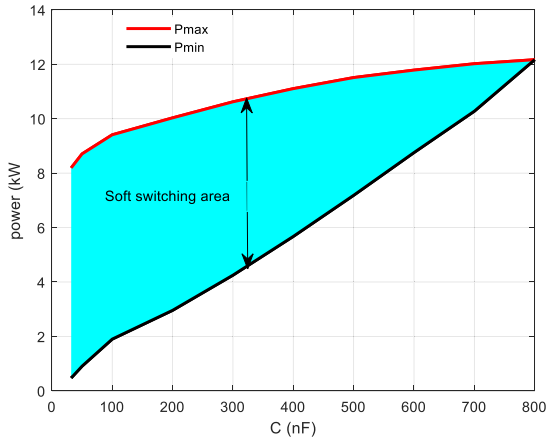

FIGURE 13. Soft switching area as a function of resonant capacitor.

TABLE 1. Simulation constants and circuit parameters.

Parameter		Symbol	Value
Rated power		P_o	8.2 kW
DC input voltage		V_i	200 V
Output voltage		V_o	600 V
Boost inductor		L_b	50 uH
Resonant capacitor		C_r	32 nF
Output capacitor		C_o	1200 uF
Load resistance (Ω)		R_o	100 Ω
Switching frequency		f_s	40 kHz
Semiconductor devices	S_1, S_2	IKY75N120CH3	
	D_1, D_2, D_o	Fast recovery diodes CS241250	

PSIM software [30] with the circuit constants and simulation specifications given in Table 1. The conversion efficiency calculation is calculated using the thermal module of the PSIM program that provides a quick way of estimating the

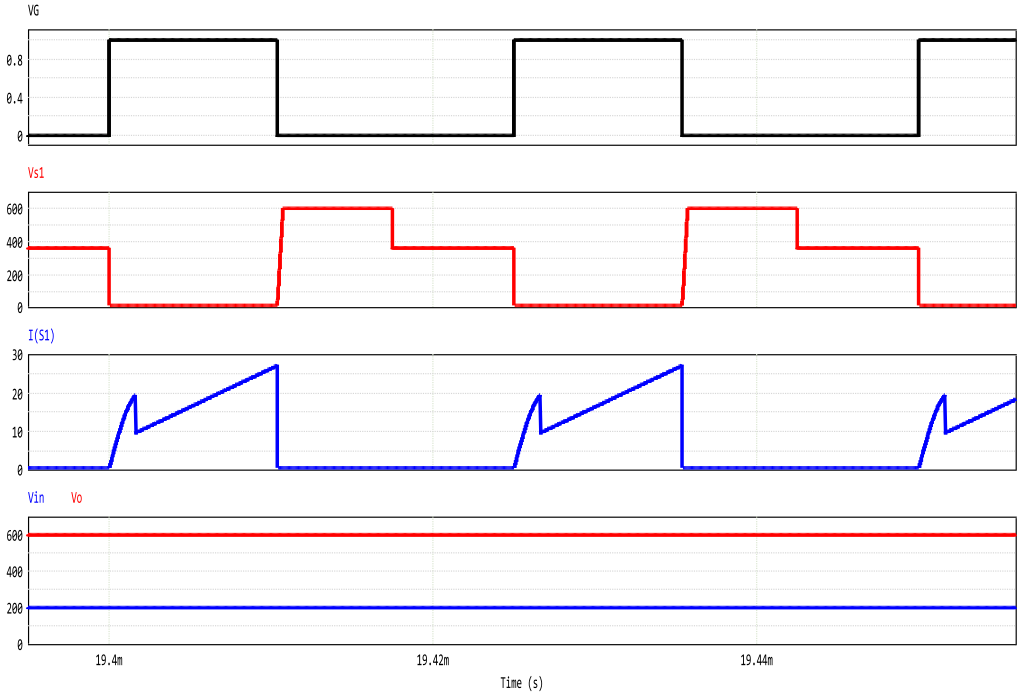

FIGURE 14. Simulation voltage and current waveforms from up to down: gating signal, active switch voltage and current, input and output voltage.

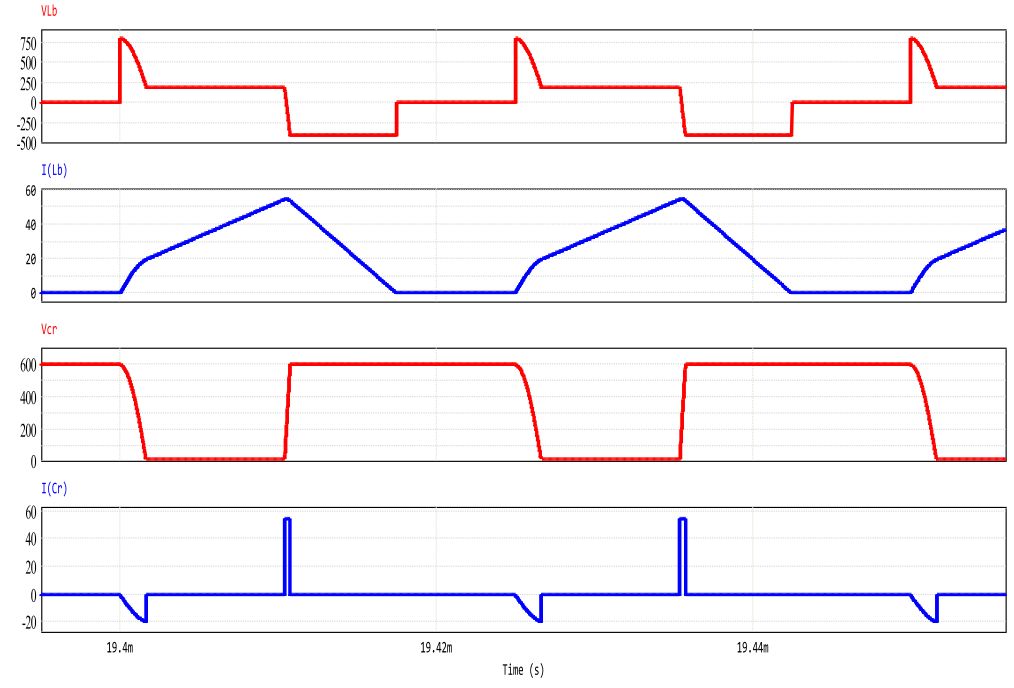

FIGURE 15. Simulation voltage and current waveforms from up to down: boost inductor voltage, boost inductor current, resonant capacitor voltage and resonant capacitor current.

losses of semiconductor devices and the core and the winding losses of inductors. The simulation results with the voltage and current waveforms are given and discussed in detail in this section.

The simulated voltage and current waveforms during one switching cycle at a switching frequency of 40 kHz are shown in Figs. 14-16. From the obtained voltage and current waveforms, it is clear to observe that the representative results

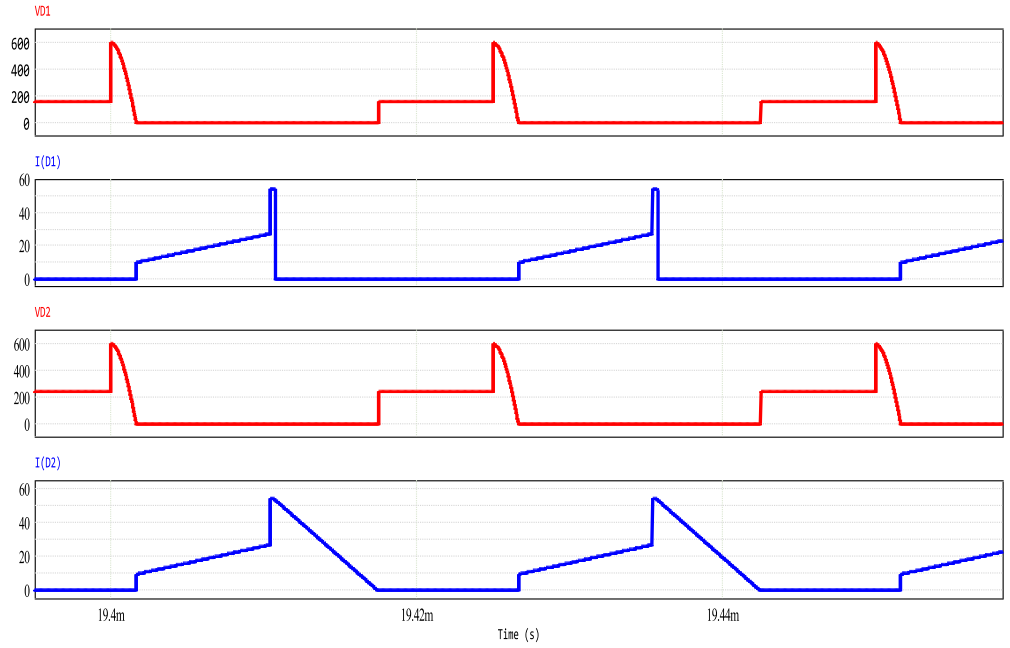

FIGURE 16. Simulation voltage and current waveforms from up to down: diode D_1 voltage, D_1 current, diode D_2 voltage and D_2 current.

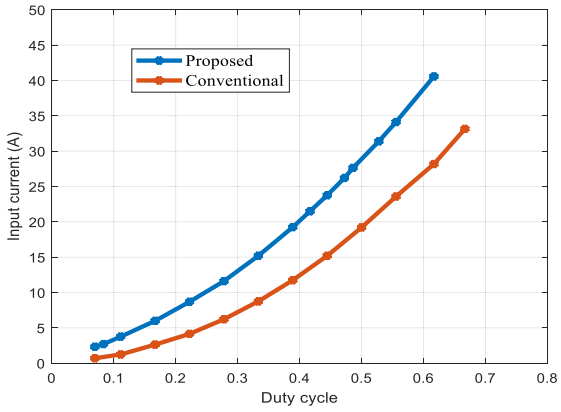

FIGURE 17. Variation of the average input current with the duty cycle.

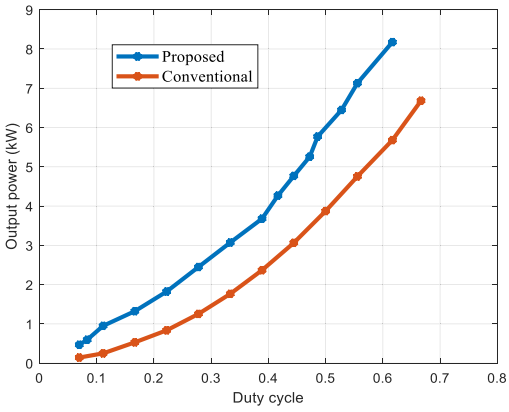

FIGURE 18. Output power regulation characteristic.

of voltage and current waveforms are in perfect agreement with the expected of Fig. 6 and the computational results shown in Fig. 9.

Fig. 17 depicts the variation of the average input current with the duty cycle of the proposed converter and the conventional hard switching boost converter.

The output power of the proposed converter is regulated by controlling the duty cycle. Fig. 18 shows the output power regulation characteristic with the soft switching operation range of the proposed converter as compared with the conventional one for the same parameter values. The proposed converter draws more current at the same duty cycles, this is because it gives more output power than the conventional one at the same working conditions. It is clear to note that the proposed converter delivers higher rated power of 8.2 kW compared to 5.72 kW of the conventional one (about 30%) at rated power condition. Efficiency comparison between the proposed soft switching and conventional boost converter is shown in Fig. 19. A stable and steady high conversion efficiency more than 97% can be obtained over a wide output power conversion range between minimum power of 460 W up to 8.2 kW with complete soft switching operation.

The efficiency comparison of Fig. 19 validates the enhanced performance of the proposed converter with the auxiliary resonant circuit over the conventional hard switching converter. This is suitable for battery charger applications since the converter is required to work from low load state to full load state. From Fig. 19, it is clear to notice that the proposed converter has a high efficiency compared to the conventional hard switching converter at low and high output power ratings. Where, as the output

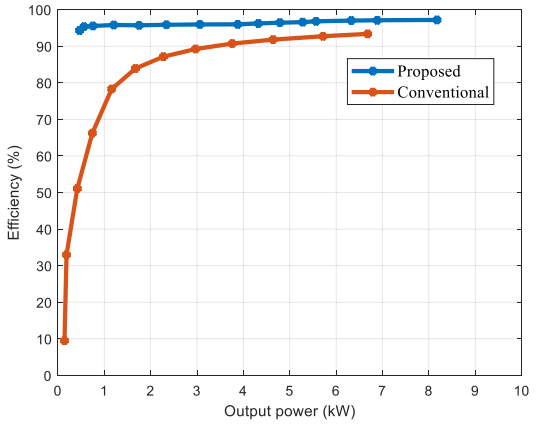

FIGURE 19. Power conversion efficiency comparison.

power consumption reduces, the duty cycle D also lessens and the turn-on time duration of the main and active switches S_1 and S_2 reduces. When the input power consumption is less than the minimum power given by (36), the voltage v_{cr} across the resonant capacitor C_r is not fully discharged to zero during Mode 1. Therefore, this residual voltage across C_r appears across the switches S_1 and S_2 at turn-off instant preventing them from complete zero voltage switching (ZVS) operation. This action produces a small overlap transition between the switch's voltages and currents waveforms at turn-off instants. As a result, increasing the switching losses and reduces the power conversion efficiency. Nevertheless, these switching power losses are much less compared to that of the hard switching operation because the residual voltage across C_r is much smaller than the voltage resulting from hard switching turn-off operation. Therefore, this turn-off can be considered a quazi-ZVS turn-off switching as shown in Fig. 20(a). On other hand, at high power above the rated power, the converter operates at continuous current mode and the turn-on switching of the active switches S_1 and S_2 occurs at a residual boost inductor current i_{Lb}. This action leads to an increase in the turn on switching losses but it still less than that of the hard switching converter. This turn-on switching can be considered a quazi-ZVS turn-on.

Fig. 21 shows the circuit configuration of proposed three phase SS-IBC using the proposed one phase converter. Figs. 22 and 23 depict the gating signal of the active switches and the input current waveforms for different duty cycles of 0.40 and 0.61, respectively. The duty cycles for all phases are equal and PWM switching function is shifted by 120°.

The ripple factor of different phases of the proposed multiphase interleaved boost converter compared to the conventional hard switching converter is illustrated in Fig. 24. It is obvious to note that the ripple factor is highly improved as the number of interleaved phases increases. The ripple factor at rated power is 1.65, 0.39 and 0.29 for the one-phase, two-phase and three-phase interleaved converters, respectively, compared to 2.33 of conventional hard switching converter.

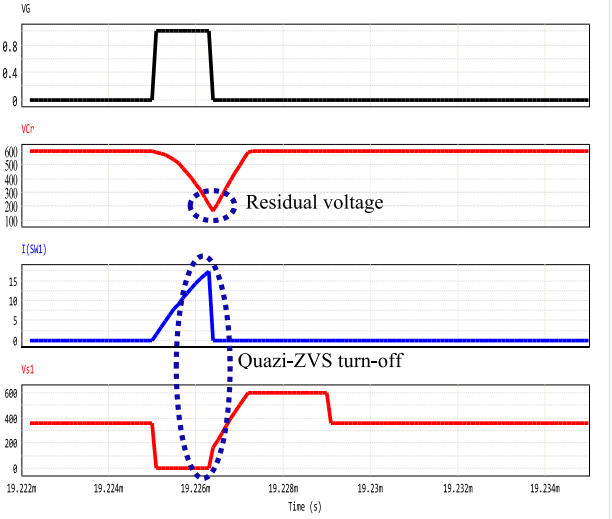

(a) Quazi-ZVS turn-off.

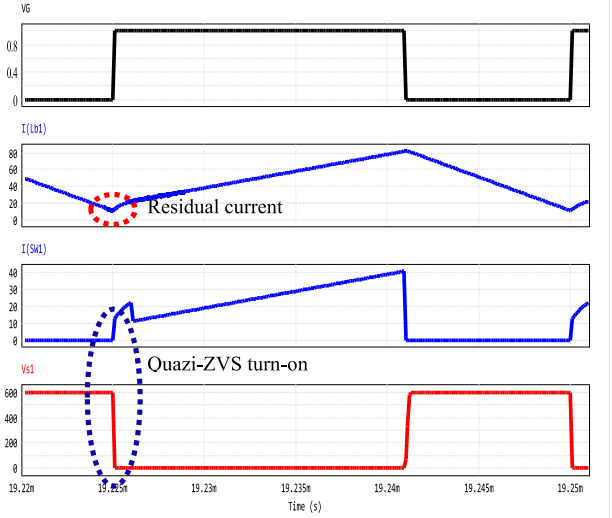

(b) Quazi-ZVS turn-on.

FIGURE 20. Quazi-soft switching of the proposed SS-IBC at turn-off and turn-on of active switches.

TABLE 2. Scaled down prototype parameters.

Parameter		Symbol	Value
Rated power		P_o	600 W
DC input voltage		V_i	40 V
Output voltage		V_o	140 V
Boost inductor		L_b	80 uH
Resonant capacitor		C_r	50 nF
Output capacitor		C_o	2200 uF
Switching frequency		f_s	25 kHz
Semiconductor devices	S_1, S_2	IPW60R070P6	
	D_1, D_2, D_o	RURG5060 ultrafast diodes	

V. EXPERIMENTAL RESULTS

In order to validate the analysis, different operation modes and the performance of the proposed SS-IBC, experimental tests were accomplished on a downsized hardware setup rated 1.0 kW due to the limitation of the Lab facilities. For the specification being considered in Table 2, Infineon

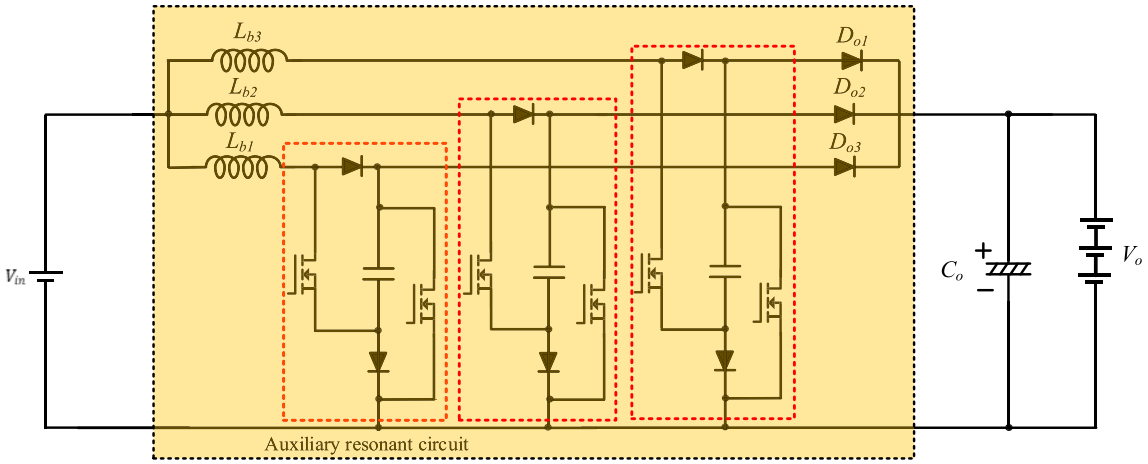

FIGURE 21. Circuit configuration of the proposed three phase SS-IBC.

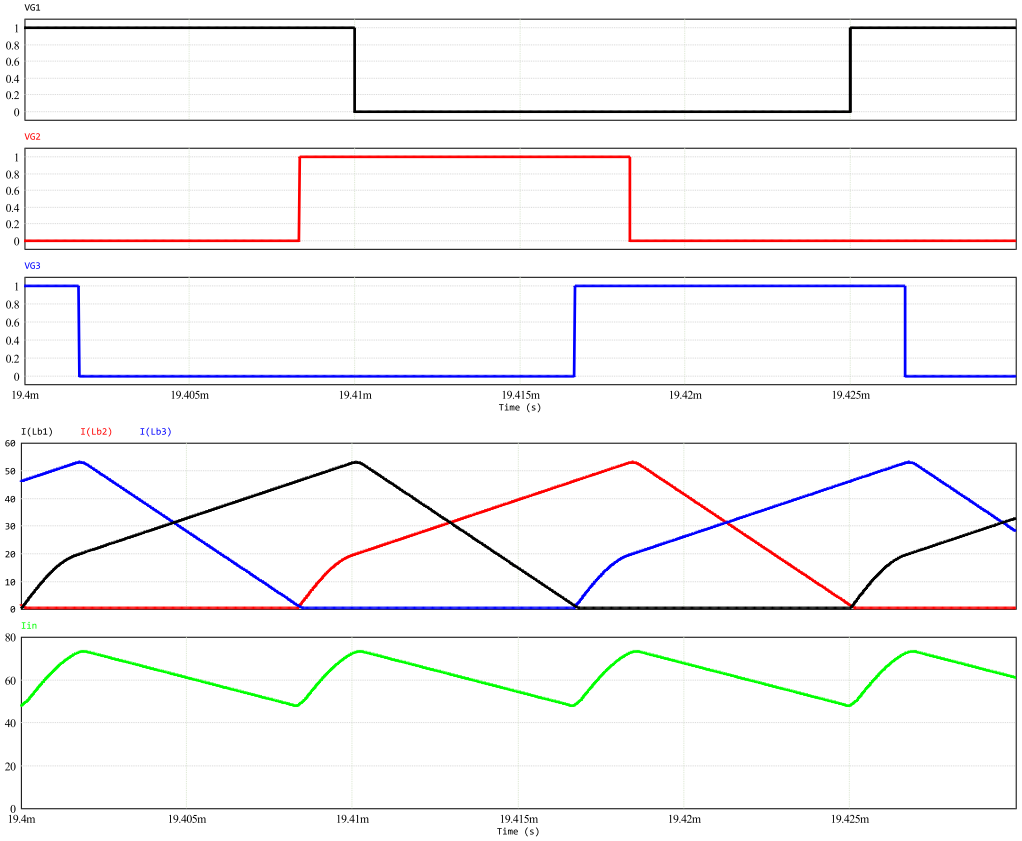

FIGURE 22. Boost inductor and input currents of proposed three phase interleaved boost converter, D = 0.40.

IPW60R070P6 MOSFETS are used for the switches S_1 and S_2. On Semiconductor RURG5060 ultrafast diodes with soft recovery characteristics are used for the diodes D_1, D_2 and D_o. The current and voltage waveforms have been recorded using Tektronix TDS 2024C digital storage oscilloscope. Fig. 25 illustrates the overall appearance of the prototype implemented in the laboratory and the parameters are given in Table 2. The experimental results are described and discussed in the following:

The experimental voltage and current waveforms for the one phase converter during two switching cycles at a switching frequency of 25 kHz are shown in Figs. 26-28. The five operation modes, which are analyzed in Section II, are identified. The gating signal, waveforms of the active switches' voltage and current and output voltage are illustrated in Fig. 25. The boost inductor voltage and current waveforms and the resonance capacitor voltage and current are shown in Fig. 26. The diodes D_1

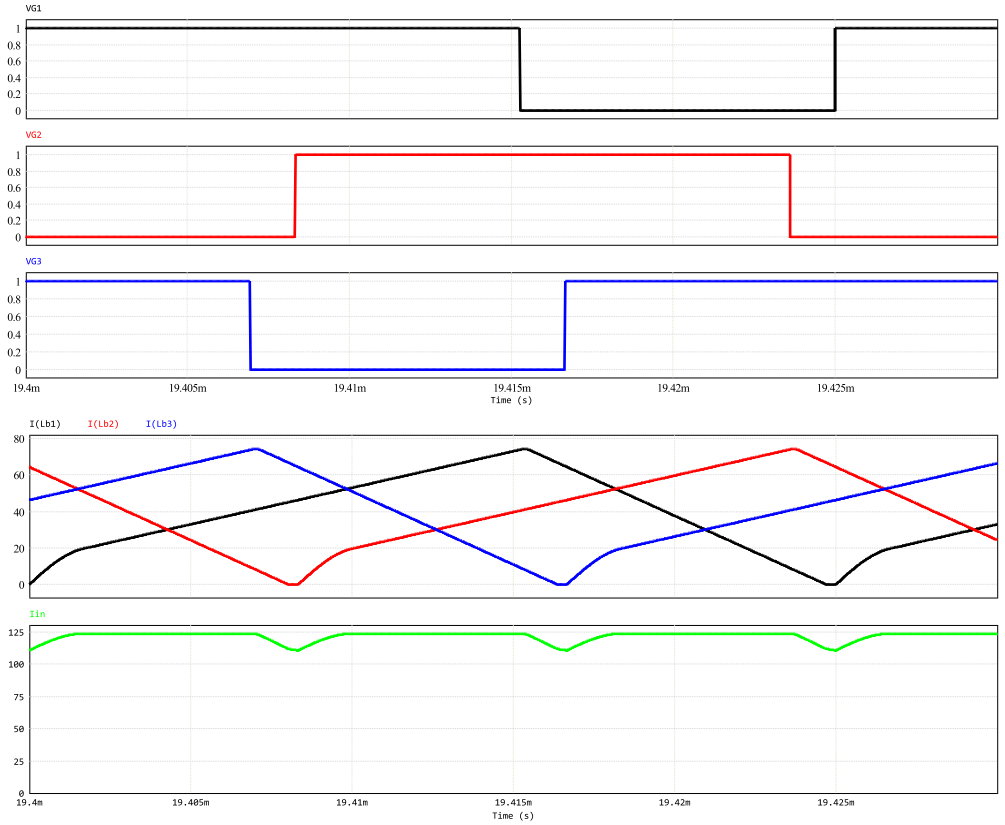

FIGURE 23. Boost inductor and input currents of proposed three phase interleaved boost converter, D = 0.61.

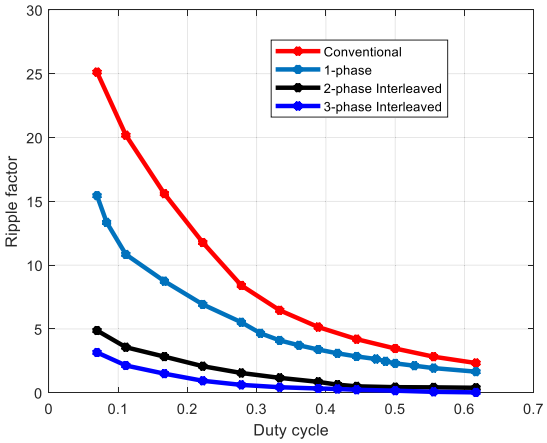

FIGURE 24. Ripple factor of input current.

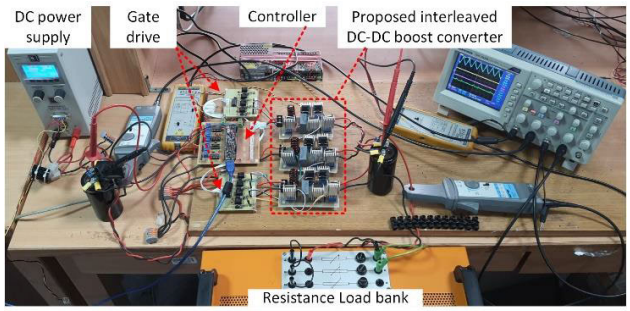

FIGURE 25. Photo of the hardware setup.

and D_2 voltage and currents waveforms are depicted in Figs 27.

Fig. 29 demonstrates the simulation results at the same circuit parameters used in the downsized hardware listed in table 2 and relevant to experimental results of Figs. 26-28. From these experimental and simulation waveforms, it is obvious that the experimental results are in perfect agreement with those of computed and simulation results given at rated power in Fig. 9 and Figs. 14-16, respectively.

The results displayed in Fig. 30 summarize the performance of the proposed three phase SS-IBC at different operation conditions of output power. The output power is simply controlled by adjusting the duty cycle D. The 120° phase shift in the in the boost inductor currents is shown in Figure 28(a), (c), (e), (g) and (h). Also, it can be observed that the converter has a continues input current. The results in Figure 28(b), (d), (f), (h) and (j) show the proposed three phase SS-IBC input voltage, input current, output voltage and output current with their associated average values at five different values of duty cycles of 0.3, (4), (45), (0.5) and (0.55), respective. These average values are used to calculate the conversion efficiency of the proposed converter at different loading levels and duty cycles (efficiency is

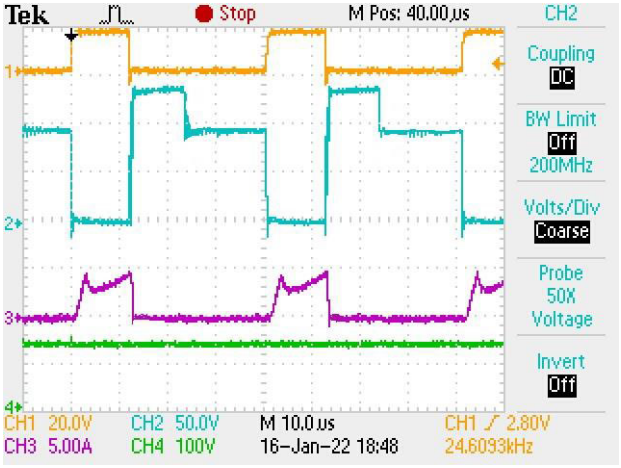

FIGURE 26. Gating signal (CH1), switches voltage, and current waveforms (CH2, CH3) and output voltage (CH4).

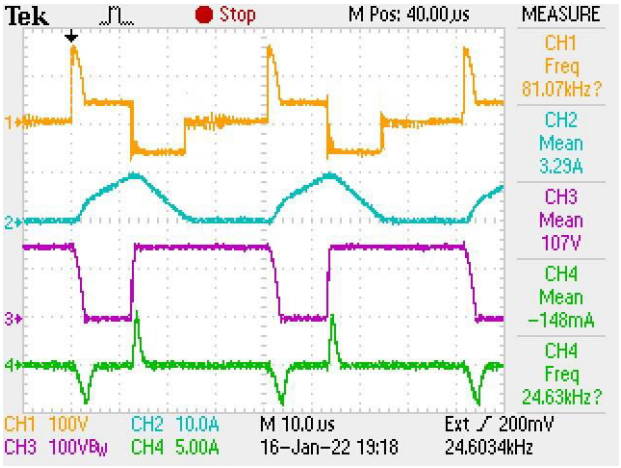

FIGURE 27. Voltages and currents of boost inductor (CH1., CH2) and resonant capacitor (CH3, CH4).

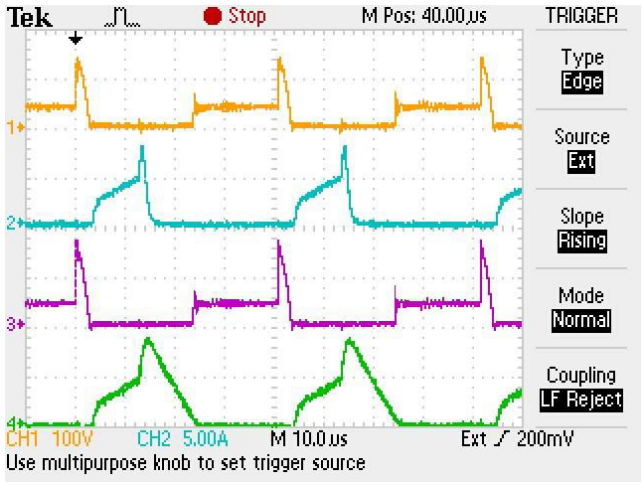

FIGURE 28. Voltages and currents of diodes D_1 (CH1, CH2) and D_2 (CH3, CH4).

95.84% at D = 0.3, 97.52% at D = 0.4, 97.57% at D = 0.45, 98.78% at D = 0.5, and 98.39% at D = 0.55). Maximum efficiency is 98.78% at power of 798 W.

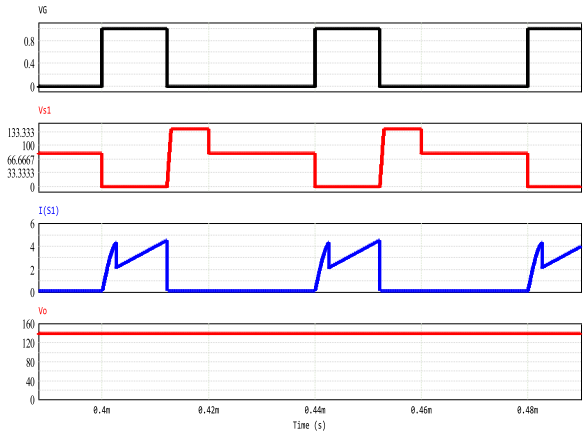

(a) Gating signal, switches voltage, current and output voltage.

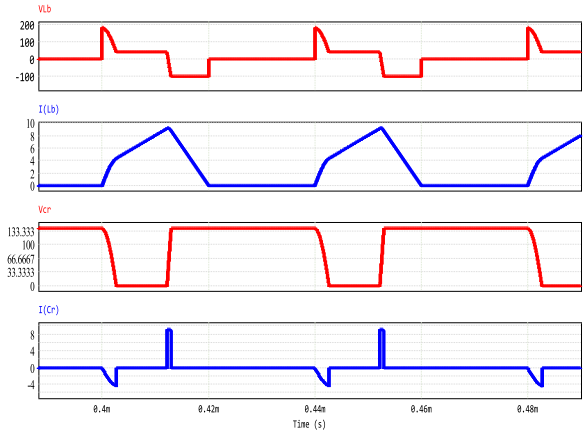

(b) Voltages and currents of boost inductor and resonant capacitor.

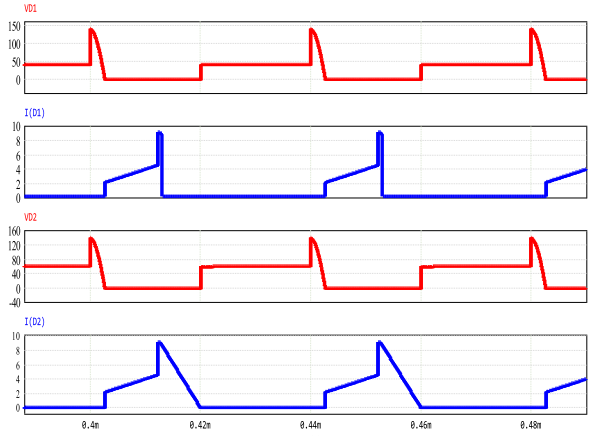

(c) Voltages and currents of diodes D_1 and D_2.

FIGURE 29. Simulation results for the downsized converter.

VI. COMPARISON WITH EXISTING TOPOLOGIES

Detailed comparison of the proposed converter with some other soft switching converters found in the most recent published work is listed in Table 3 in terms of topology, number of used devices as compared to the conventional hard switching converter, input voltage, output voltage, rated power, switching frequency and conversion efficiency. It is depicted that; the proposed converter has a lesser number of

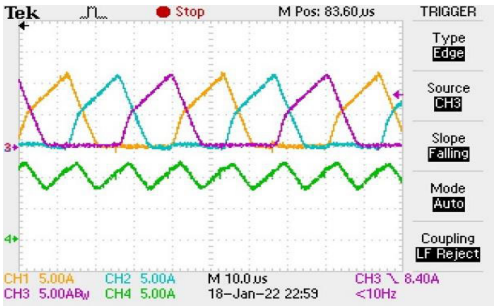

(a) Boost inductor currents (CH1, CH2 and CH3) and input current (CH4) of proposed three phase SS-IBC, D = 0.3.

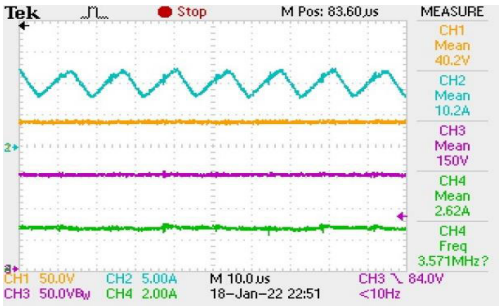

(b) Input voltage and current (CH1, CH2), output voltage and current (CH3, CH4), D=0.3.

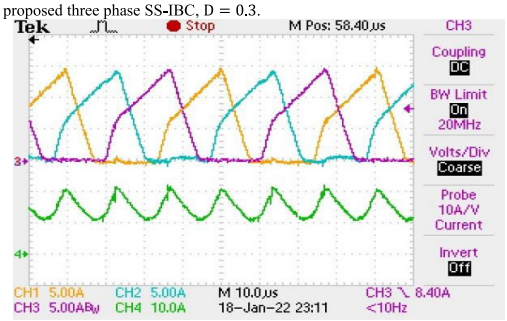

(c) Boost inductor currents (CH1, CH2 and CH3) and input current (CH4) of proposed three phase SS-IBC, D = 0.4.

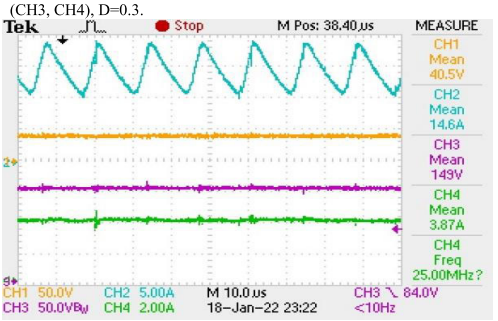

(d) Input voltage and current (CH1, CH2), output voltage and current (CH3, CH4), D=0.4.

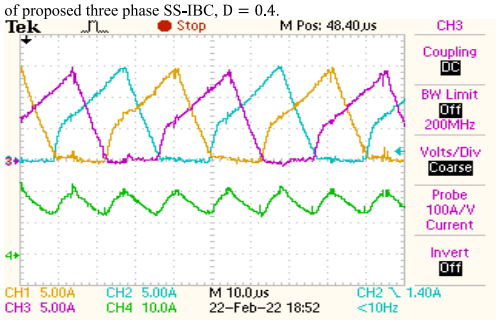

(e) Boost inductor currents (CH1, CH2 and CH3) and input current (CH4) of proposed three phase SS-IBC, D = 0.45.

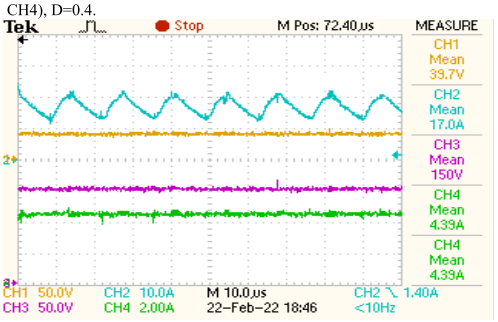

(f) Input voltage and current (CH1, CH2), output voltage and current (CH3, CH4), D=0.45.

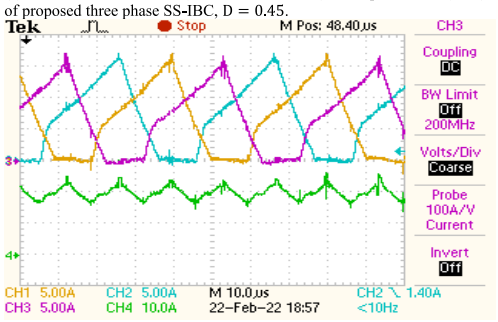

(g) Boost inductor currents (CH1, CH2 and CH3) and input current (CH4) of proposed three phase SS-IBC, D = 0.5.

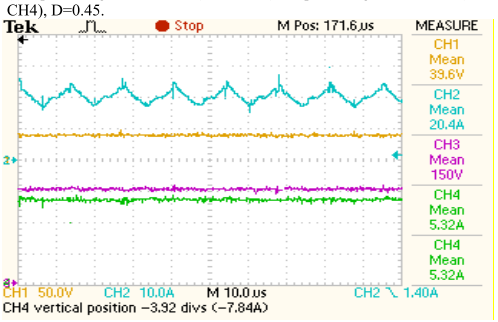

(h) Input voltage and current (CH1, CH2), output voltage and current (CH3, CH4), D=0.5.

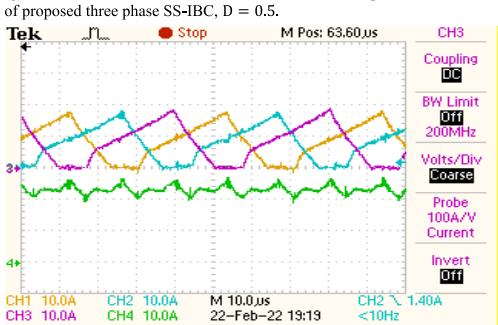

(i) Boost inductor currents (CH1, CH2 and CH3) and input current (CH4) of proposed three phase SS-IBC, D = 0.55.

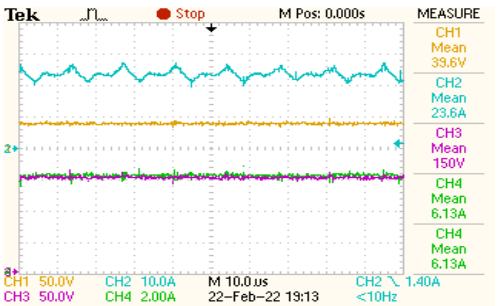

(j) Input voltage and current (CH1, CH2), output voltage and current (CH3, CH4), D=0.55.

FIGURE 30. Experimental current and voltage waveforms summarize the performance of the proposed three-phase SS-IBC at different operation points.

TABLE 3. Comparison between the proposed soft switching converter with some other soft switching converters.

Ref. no.	Topology	Devices				Operation conditions				No. of Operation Modes	Max. Eff. %
		L	C	D	S	V_{in}	V_0	P_0 (kW)	f_{sw} (kHz)		
Proposed	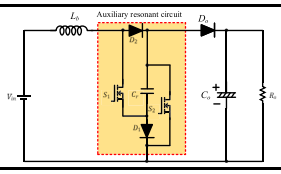	**1**	**1**	**2**	**2**	**200**	**600**	**8.2**	**40**	**5**	**98.78**
Shamsi [31], (2021)	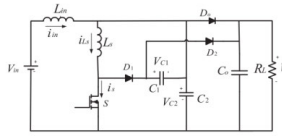	2	3	3	1	48	96	0.22	100	7	97.6
Tran [32], (2020)	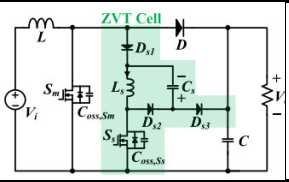	2	3	6	2	150	400	2	100	11	98.02
Jung [38], (2011)	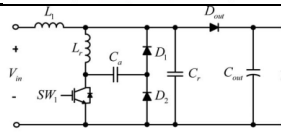	2	2	2	1	200	400	1.2	30	8	97.8
Rodriguez, [34], (2019)	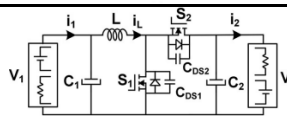	1	3	2	2	400	800	10	20	-	97.5
Musbahu [9] , (2017)	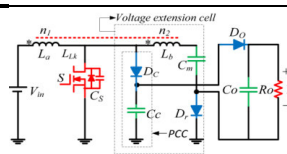	1	2	2	1	20	190	0.25	50	5	93.5
Esteki [35], 2017)	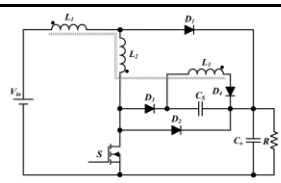	3	2	4	1	50	100	0.2	100	7	95.8
Saravanan [36], (2017)	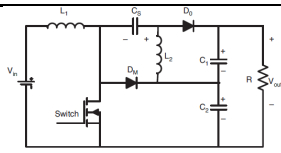	2	3	2	1			0.1	24	4	92.5
Eom [37], (2012)	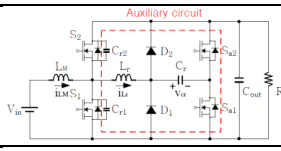	2	3	6	4	200	400	1.0	30	9	96.15
Tseng [33], (2011)	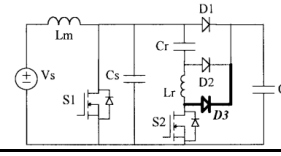	2	3	4	2	200	400	0.75	80	8	95%

components and superior efficiency as compared to the other converters.

Fig. 31 illustrates the efficiency comparison of the proposed soft switching converter with the other soft switching

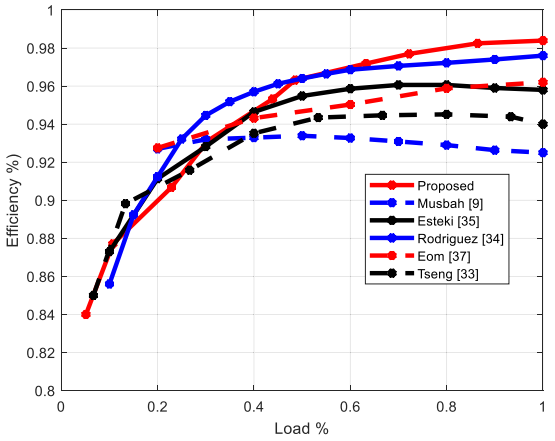

FIGURE 31. Efficiency comparison of the proposed converter with other converters at different load conditions.

converters at different output power range. Since the power ratings of each converter are different as shown in Table 3, the efficiency comparison is done in terms of thee normalized output as a percentage of the rated output power of each converter. It can be noted that the proposed converter has a superior efficiency characteristic among the other converters in a wide output power range.

VII. CONCLUSION

A soft switching multiphase SS-IBC working in discontinuous current mode with high voltage gain using auxiliary resonant circuit for EV applications is presented in this paper. Operation principles, detailed analysis, voltage and current waveforms and performance evaluation have been investigated through simulation and experimental results. The input current is equally divided along two parallel phases and consequently the current stress on the controlled switches and the conduction losses are considerably reduced. Turning on and off of the switches can be achieved at ZCS and ZVS, respectively and overall efficiency of the proposed converter has been improved. Due to the soft switching operation of the main and auxiliary switches in a wide output power control range, the proposed converter has lower switching losses and consequently high conversion efficiency compared to the standard hard switching boost converter. High conversion efficiency more than 97% has been obtained in simulation for a wide output power range of 8.2 kW to minimum power of 460 and the.

The converter performance is also validated experimentally on a downsized hardware rated 1.0 kW and the maximum efficiency is found to be 98.78%. The proposed SS-IBC can be considered as a cost effective retrofit for chargers and high voltage battery in EV applications.

REFERENCES

[1] N. A. Ahmed and F. M. Alhuwaishel, "Solar powered unmanned aerial vehicle with active output filter under non-linear load conditions," *IEEE Access*, vol. 9, pp. 77212–77228, 2021, doi: 10.1109/ACCESS.2021.3083092.

[2] R. Vidhi, P. Shrivastava, and A. Parikh, "Social and technological impact of businesses surrounding electric vehicles," *Clean Technol.*, vol. 3, no. 1, pp. 81–97, Feb. 2021, doi: 10.3390/cleantechnol3010006.

[3] S. Wappelhorst, "Update on government targets for phasing out new sales of internal combustion engine passenger cars," in *Proc. Int. Council Clean Transp.*, Jul. 2021, pp. 1–12. [Online]. Available: https://theicct.org/sites/default/files/publications/update-govt-targets-ice-phaseouts-jun2021_0.pdf

[4] A. Poorfakhraei, M. Narimani, and A. Emadi, "A review of multilevel inverter topologies in electric vehicles: Current status and future trends," *IEEE Open J. Power Electron.*, vol. 2, pp. 155–170, 2021, doi: 10.1109/OJPEL.2021.3063550.

[5] M. Ehsani, K. M. Rahman, M. D. Bellar, and A. J. Severinsky, "Evaluation of soft switching for EV and HEV motor drives," *IEEE Trans. Ind. Electron.*, vol. 48, no. 1, pp. 82–90, Feb. 2001.

[6] S. Habib, M. M. Khan, F. Abbas, and H. H. Tang, 'Assessment of electric vehicles concerning impacts, charging infrastructure with unidirectional and bidirectional chargers, and power flow comparisons," *Int. J. Energy Res.*, vol. 42, no. 11, pp. 3416–3441, 2018, doi: 10.1002/er.4033.

[7] M. R. Khalid, I. A. Khan, S. Hameed, M. S. J. Asghar, and J.-S. Ro, "A comprehensive review on structural topologies, power levels, energy storage systems, and standards for electric vehicle charging stations and their impacts on grid," *IEEE Access*, vol. 9, pp. 128069–128094, 2021, doi: 10.1109/ACCESS.2021.3112189.

[8] A. Nabil Ahmed and J. Y. Madouh, "High-frequency full-bridge isolated DC-DC converter for fuel cell power generation systems," *Electr. Eng.*, vol. 100, pp. 239–251, Oct. 2018, doi: 10.1007/s00202-016-0499-6.

[9] M. Muhammad, M. Armstrong, and M. A. Elgendy, "Analysis and implementation of high-gain non-isolated DC–DC boost converter," *IET Power Electron.*, vol. 11, pp. 1241–1249, Oct. 2017, doi: 10.1049/iet-pel.2016.0810.

[10] O. Lopez-Santos, J. C. Mayo-Maldonado, J. C. Rosas-Caro, J. E. Valdez-Resendiz, D. A. Zambrano-Prada, and O. F. Ruiz-Martinez, "Quadratic boost converter with low-output-voltage ripple," *IET power Electron.*, vol. 13, no. 8, pp. 1605–1612, Jun. 2020, doi: 10.3390/electronics9091480.

[11] P. Luo, L. Guo, J. Xu, and X. Li, "Analysis and design of a new non-isolated three-port converter with high voltage gain for renewable energy applications," *IEEE Access*, vol. 9, pp. 115909–115921, 2021, doi: 10.1109/ACCESS.2021.3106058.

[12] T. Chaudhury and D. Kastha, "A high gain multiport DC–DC converter for integrating energy storage devices to DC microgrid," *IEEE Trans. Power Electron.*, vol. 35, no. 10, pp. 10501–10514, Oct. 2020, doi: 10.1109/TPEL.2020.2977909.

[13] G. Zhou, Q. Tian, and L. Wang, "Soft-switching high gain three-port converter based on coupled inductor for renewable energy system applications," *IEEE Trans. Ind. Electron.*, vol. 69, no. 2, pp. 1521–1536, Feb. 2022, doi: 10.1109/TIE.2021.3060614.

[14] K.-C. Tseng, C.-C. Huang, and C.-A. Cheng, "A high step-up converter with voltage-multiplier modules for sustainable energy applications," *IEEE J. Emerg. Sel. Topics Power Electron.*, vol. 3, no. 4, pp. 1100–1108, Dec. 2015, doi: 10.1109/TPEL.2012.2217157.

[15] M. Moradzadeh, S. Hamkari, E. Zamiri, and R. Barzegarkhoo, "Novel high step-up DC/DC converter structure using a coupled inductor with minimal voltage stress on the main switch," *J. Power Electron.*, vol. 16, no. 6, pp. 2005–2015, Nov. 2016, doi: 10.6113/JPE.2016.16.6.2005.

[16] H. Zhu, D. Zhang, B. Zhang, and Z. Zhou, "A non-isolated three-port DC–DC converter and three-domain control method for PV-battery power systems," *IEEE Trans. Ind. Electron.*, vol. 62, no. 8, pp. 4937–4947, Apr. 2015. [Online]. Available: http://ieeexplore.ieee.org/document/7014280/

[17] T. Cheng, D. D. Lu, A. Gong, and D. Verstraete, "Analysis of a three-port DC-DC converter for PV-battery system using DISO boost and SISO buck converters," in *Proc. Australas. Univ. Power Eng. Conf. (AUPEC)*, Wollongong, NSW, Australia, 2015, pp. 1–6. [Online]. Available: http://ieeexplore.ieee.org/ document/7324842/

[18] K. J. Reddy and N. Sudhakar, "High voltage gain interleaved boost converter with neural network based MPPT controller for fuel cell based electric vehicle applications," *IEEE Access*, vol. 6, pp. 3899–3908, 2018, doi: 10.1109/ACCESS.2017.2785832.

[19] D. Wang, Z. Wang, Z. Peng, Y. Zhang, and X.-F. Cheng, "A four-phase interleaved buck-boost converter with changed load connection for the fuel cell activation," *IEEE Access*, vol. 9, pp. 102104–102113, 2021, doi: 10.1109/ACCESS.2021.3098063.

[20] D. Guilbert, A. Gaillard, A. N'Diaye, and A. Djerdir, "Energy efficiency and fault tolerance comparison of DC/DC converters topologies for fuel cell electric vehicles," in *Proc. IEEE Transp. Electrific. Conf. Expo. (ITEC)*, Dearborn, MI, USA, 2013, pp. 1–7, doi: 10.1109/ITEC.2013.6574513.
[21] A. Garrigás, J. M. Blanes, and J. L. Lizên, "Non-isolated multiphase boost converter for a fuel cell with battery backup power system," *Int. J. Hydrogen Energy*, vol. 36, no. 1, pp. 6259–6268, May 2011, doi: 10.1016/j.ijhydene.2011.01.153.
[22] T. Mishima, Y. Takeuchi, and M. Nakaoka, "Analysis, design, and performance evaluations of an edge-resonant switched capacitor cell-assisted soft-switching PWM boost DC–DC converter and its interleaved topology," *IEEE Trans. Power Electron.*, vol. 28, no. 7, pp. 3363–3378, Jul. 2013, doi: 10.1109/TPEL.2012.2227504.
[23] J. Choi, H. Cha, and B.-M. Han, "A three-phase interleaved DC–DC converter with active clamp for fuel cells," *IEEE Trans. Power Electron.*, vol. 25, no. 8, pp. 2115–2123, Aug. 2010, doi: 10.1109/TPEL.2010.2045659.
[24] M. Muhammad, M. Armstrong, and M. A. Elgendy, "A non-isolated interleaved boost converter for high voltage gain applications," *IEEE J. Emerg. Sel. Topics Power Electron.*, vol. 4, no. 2, pp. 352–362, Jun. 2015, doi: 10.1109/JESTPE.2015.2488839.
[25] H. Saleeb, K. Sayed, and A. R. Kassem Mostafa, "Control and analysis of bidirectional interleaved hybrid converter with coupled inductors for electric vehicle applications," *Electr. Eng.*, vol. 102, pp. 195–222, Oct. 2020, doi: 10.1007/s00202-019-00860-3.
[26] A. Garg and M. Das, "High efficiency three phase interleaved buck converter for fast charging of EV," in *Proc. 1st Int. Conf. Power Electron. Energy (ICPEE)*, 2021, pp. 1–5, doi: 10.1109/ICPEE50452.2021.9358486.
[27] J. Wang, "An efficiency optimization control method for three-phase interleaved DC–DC converter," in *Proc. 3rd Asia Energy Electr. Eng. Symp. (AEEES)*, 2021, pp. 285–289, doi: 10.1109/AEEES51875.2021.9403039.
[28] S. Amir Sayed Fatahi, M. Esteki, and H. Farzanehfard, "A soft switching interleaved high step-down converter with low voltage stress," in *Proc. 12th Power Electron., Drive Syst., Technol. Conf. (PEDSTC)*, Feb. 2021, pp. 1–6, doi: 10.1109/PEDSTC52094.2021.9405943.
[29] D. Amani, R. Beiranvand, and M. Zolghadri, "A new high step-up interleaved LLC converter," in *Proc. 12th Power Electron., Drive Syst., Technol. Conf. (PEDSTC)*, 2021, pp. 1–6, doi: 10.1109/PEDSTC52094.2021.9405945.
[30] *Power Electronics Simulations*, Powersim Technology, Vancouver, BC, Canada, 2021. [Online]. Available: https://www.powersimtech.com
[31] T. Shamsi, M. Delshad, E. Adib, and M. R. Yazdani, "A new simplestructure passive lossless snubber for DC–DC boost converters," *IEEE Trans. Ind. Electron.*, vol. 68, no. 3, pp. 2207–2214, Mar. 2021, doi: 10.1109/TIE.2020.2973906.
[32] H. N. Tran and S. Choi, "A family of ZVT DC–DC converters with low-voltage ringing," *IEEE Trans. Power Electron.*, vol. 35, no. 1, pp. 59–69, Jan. 2020, doi: 10.1109/TPEL.2019.2911040.
[33] C.-J. Tseng and C.-L. Chen, "Novel ZVT-PWM converters with active snubbers," *IEEE Trans. Power Electron.*, vol. 13, no. 5, pp. 861–869, Sep. 1998, doi: 10.1109/63.712292.
[34] A. Rodriguez, A. Vazquez, M. R. Rogina, and F. Briz, "Synchronous boost converter with high efficiency at light load using QSW-ZVS and SiC mosfets," *IEEE Trans. Ind. Electron.*, vol. 65, no. 1, pp. 386–393, Jan. 2018, doi: 10.1109/TIE.2017.2716864.
[35] M. Esteki, M. Mohammadi, M. R. Yazdani, E. Adib, and H. Farzanehfard, "Family of soft-switching pulse-width modulation converters using coupled passive snubber," *IET Power Electron.*, vol. 10, no. 7, pp. 792–800, Jun. 2017, doi: 10.1049/iet-pel.2016.0362.
[36] S. Saravanan and N. R. Babu, "A modified high step-up non-isolated DC–DC converter for PV application," *J. Appl. Res. Technol.*, vol. 15, no. 3, pp. 242–249, Jun. 2017, doi: 10.1016/j.jart.2016.12.008.
[37] J. K. Eom, J. G. Kim, J. H. Kim, S. T. Oh, Y. C. Jung, and C. Y. Won, "Analysis of a novel soft switching bidirectional DC–DC converter," *J. Power Electron.*, vol. 12, no. 6, pp. 859–869, Nov. 2012, doi: 10.6113/JPE.2012.12.6.859.
[38] D. Jung, Y. Ji, S. Park, Y. Jung, and C. Won, "Interleaved soft-switching boost converter for photovoltaic power-generation system," *IEEE Trans. Power Electron.*, vol. 26, no. 4, pp. 1137–1145, Apr. 2011, doi: 10.1109/TPEL.2010.2090948.

NABIL A. AHMED (Senior Member, IEEE) received the B.Sc. and M.Sc. degrees from the Electrical and Electronics Engineering Department, Assiut University, Egypt, and the Ph.D. degree from the University of Toyama, Japan, in 1989, 1994, and 2000, respectively, all in electrical engineering. In 1989, he joined Assiut University, where he has been a Professor, since 2011. He was a Postdoctoral Fellow at the Electrical Engineering Saving Research Center, Kyungnam University, South Korea, from October 2004 to April 2005, and a JSPS Postdoctoral Fellow at Sophia University, Japan, from July 2005 to September 2006. Currently, he is an Associate Professor with the Electrical Engineering Department, College of Technological Studies, Public Authority of Applied Education and Training, Kuwait (on leave from Assiut University). His research interests include power electronics applications, variable speed drives, soft-switching converters, renewable energy systems, and its integration to electric power grid. He was a recipient of the Egypt State Encouraging of Research Prize 2005, the Japan Monbusho Scholarship, from 1996 to 2000, the JSPS Fellowship, from 2005 to 2007, the Best Paper Awards from ICEMS'05 and IATC'06 Conferences, and the Best Presentation Award from ICEMS'04 Conference. He has been listed in *Marque's Who is Who in the World*, since 2009. He is a Senior Member of the IEEE Industrial Electronics Society.

BADER N. ALAJMI (Member, IEEE) received the B.Sc. and M.Sc. degrees from California State University, Fresno, in 2001 and 2006, respectively, and the Ph.D. degree in power electronics from the University of Strathclyde, Glasgow, U.K., in 2013. Currently, he is an Assistant Professor with the College of Technological Studies, Public Authority of Applied Education and Training, Kuwait. His research interests include digital control of power electronic systems, micro-grids and distributed generation, and renewable energy

IBRAHIM ABDELSALAM (Senior Member, IEEE) received the B.Sc. and M.Sc. degrees (Hons.) in electrical engineering from the Arab Academy for Science, and Technology and Maritime Transport, Egypt, in 2006 (Alexandria campus) and 2009 (Cairo campus), respectively, and the Ph.D. degree in power electronics from the University of Strathclyde, Glasgow, U.K., in 2016. Currently, he is a Lecturer with the Electrical Department, Academy for Science and Technology and Maritime Transport. His research interests include power electronic converters and their applications in wind energy conversion systems and advanced control strategies of the multilevel voltage and current source converters.

MOSTAFA I. MAREI (Senior Member, IEEE) received the B.Sc. and M.Sc. degrees (Hons.) from Ain Shams University, Cairo, Egypt, in 1997 and 2000, respectively, and the Ph.D. degree from the University of Waterloo, Waterloo, ON, Canada, in 2004, all in electrical engineering. From 2004 to 2006, he was a Postdoctoral Fellow at the University of Waterloo. Currently, he is a Professor with the Department of Electrical Power and Machines, Ain Shams University. His research interests include power electronics, distributed and renewable generation, micro-grids, power quality, custom power, electrical drives, and artificial intelligent applications in power systems. He received the State Incentive Award in Engineering Sciences from the Academy of Scientific Research and Technology, Egypt. His biography is listed in *Marque's Who is Who in the World*.